Glassy Dynamics in Condensed Isolated Polymer Chains

Martin Tress *et al.*

Science **341**, 1371 (2013);
DOI: 10.1126/science.1238950

Science (print ISSN 0036-8075; online ISSN 1095-9203) is published weekly, except the last week in December, by the American Association for the Advancement of Science, 1200 New York Avenue NW, Washington, DC 20005.

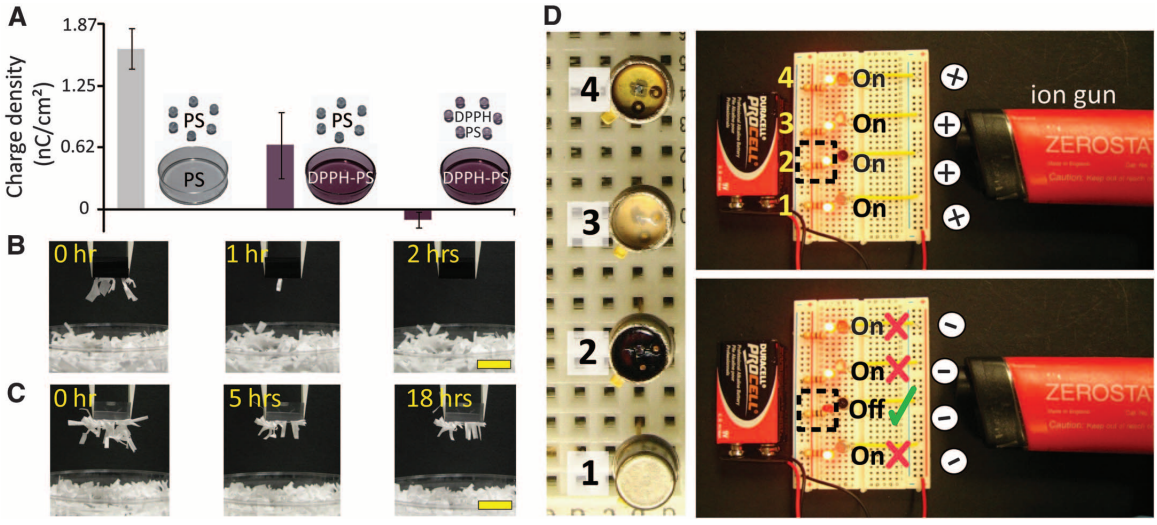

Fig. 3. Applications of antistatic polymers based on radical scavenging. (**A**) For PS beads contact-charged by shaking in PS petri dishes, the average density of charge decreases as one (middle) or both (right) of the contacting materials are doped with DPPH. Error bars correspond to standard deviations of the charges on 25 beads used in each experiment. See fig. S10 for analogous experiments with other materials. (**B**) PDMS block-doped with 1 mM of DPPH contact-charged against PS to 0.75 nC/cm^2 attracts much less small shreds and "de-dusts" completely within ~1 hour, compared with undoped PDMS piece in (C). (**C**) An equally shaped and charged PDMS piece holds paper shreds for more than a day. Scale bar, 1 cm. (**D**) An electronic circuit (for scheme, see fig. S11) in which only transistor #2 (with cap removed and with the gate covered with PS/DPPH) is undamaged (see fig. S11D) after exposure to electrostatic discharge from an ion gun.

same degree retains static electricity and paper shreds for more than a day (Fig. 3C).

Arguably, the most impactful application of the charge-radical regulation is illustrated in Fig. 3D. There, PS doped with DPPH is used to protect electronic components from failure due to electrostatic discharge, which is a ubiquitous problem in the microelectronics industry, damaging semiconductor-based devices (either upon direct contact or arcing) and resulting in losses currently measured in billions of dollars per year (*5*). The circuit shown comprises n-channel junction field-effect transistors (JFETs) (2N 4861A, Solitron Devices) connected serially to light-emitting diodes (LEDs). When exposed to consecutive positive/negative cycles of electrostatic/corona discharge from an electrostatic gun, the LEDs connected to undamaged transistors go cyclically "on" and "off." If, however, the accumulation of static electricity on the gate damages the transistor, its associated LED should always be "on" (*23*). In our circuit, we used four types of transistors: #1 was an intact JFET; #2 was a JFET with the metal shield removed but with the gate covered with a ~200- to 500-μm-thick layer of PS doped with 1.8% w/w DPPH; #3 had the shield removed, but the gate was covered with pure PS; and #4 had the shield removed with no polymer on the gate. As shown in Fig. 3D, the ion gun causes the damage of all transistors but #2, for which DPPH helps scavenge the radicals produced by corona discharge, thus destabilizing the accumulated charges and preventing the build-up of static electricity to damaging levels (see fig. S11 and, for additional experiments, fig. S12). Because similar effects are observed with other types of polymers and scavengers we studied—notably, the edible and biocompatible vitamin E—our results can herald a general, technically straightforward and environmentally "green" way of protecting electronics of various types from the untoward effects of static electricity.

References and Notes

1. T. Shinbrot, T. S. Komatsu, Q. Zhao, *Europhys. Lett.* **83**, 24004 (2008).
2. W. D. Greason, *IEEE Trans. Ind. Appl.* **IA-23**, 205–216 (1987).
3. N. Gibson, *J. Electrost.* **40-41**, 21–30 (1997).
4. S. T. Lai, *Spacecraft Charging: Progress in Astronautics and Aeronautics, Vol. 237* (American Institute of Aeronautics and Astronautics, Reston, VA, 2011).
5. M. Angelopoulos, *IBM J. Res. Develop.* **45**, 57–75 (2001).
6. A. Volta, *Philos. Trans. R. Soc. London* **90**, 403–431 (1800).
7. D. J. Lacks, *Angew. Chem. Int. Ed.* **51**, 6822–6823 (2012).
8. M. Tolinski, *Additives for Polyolefins: Getting the Most out of Polypropylene, Polyethylene and TPO* (Elsevier, Oxford, 2009), pp. 79–91.
9. H. T. Baytekin *et al.*, *Science* **333**, 308–312 (2011).
10. H. T. Baytekin, B. Baytekin, J. T. Incorvati, B. A. Grzybowski, *Angew. Chem. Int. Ed.* **51**, 4843–4847 (2012).
11. B. Baytekin, H. T. Baytekin, B. A. Grzybowski, *J. Am. Chem. Soc.* **134**, 7223–7226 (2012).
12. W. R. Salaneck, A. Paton, *J. Appl. Phys.* **47**, 144 (1976).
13. T. A. L. Burgo *et al.*, *Langmuir* **28**, 7407–7416 (2012).
14. M. Williams, *AIP Adv.* **2**, 010701 (2012).
15. J. Lowell, A. C. Rose-Innes, *Adv. Phys.* **29**, 947–1023 (1980).
16. L. B. Loeb, *Electrical Coronas* (Univ. of California, Berkeley, 1965).
17. Materials and methods are available as supplementary materials on *Science* Online.
18. M. Miyasaka, Y. Saito, H. Nishide, *Adv. Funct. Mater.* **13**, 113–117 (2003).
19. M. J. Waltman, P. Dwivedi, H. H. Hill Jr., W. C. Blanchard, R. G. Ewing, *Talanta* **77**, 249–255 (2008).
20. M. Kuzuya, J. Niwa, H. Ito, *Macromolecules* **26**, 1990–1995 (1993).
21. D. H. Solomon, J. D. Swift, *J. Polym. Sci. A* **3**, 3107–3116 (1965).
22. J. J. Orlando, G. S. Tyndall, *Chem. Soc. Rev.* **41**, 6294–6317 (2012).
23. S. H. Voldman, *ESD Failure Mechanisms and Models* (Wiley, Chichester, UK, 2009).

Acknowledgments: This work was supported by the Non-Equilibrium Energy Research Center (NERC), which is an Energy Frontier Research Center funded by the U.S. Department of Energy, Office of Science, Office of Basic Energy Sciences under award DE-SC0000989. T.M.H. acknowledges a grant from the Human Frontier Science Program. We thank T. Aytun for help in measuring transistor characteristics.

Supplementary Materials

www.sciencemag.org/content/341/6152/1368/suppl/DC1
Materials and Methods
Supplementary Text
Figs. S1 to S14
Reference (*24*)

3 June 2013; accepted 14 August 2013
10.1126/science.1241326

Glassy Dynamics in Condensed Isolated Polymer Chains

Martin Tress,[1] Emmanuel U. Mapesa,[1] Wilhelm Kossack,[1] Wycliffe K. Kipnusu,[1] Manfred Reiche,[2] Friedrich Kremer[1]*

In the course of miniaturization down to the nanometer scale, much remains unknown concerning how and to what extent the properties of materials are changed. To learn more about the dynamics of condensed isolated polymer chains, we used broadband dielectric spectroscopy and a capacitor with nanostructured electrodes separated by 35 nanometers. We measured the dynamic glass transition of poly(2-vinylpyridine) and found it to be bulk-like; only segments closer than 0.5 nanometer to the substrate were weakly slowed. Our approach paves the way for numerous experiments on the dynamics of isolated molecules.

Many applications in modern technology (e.g., photoresists, sensors for drug delivery, batteries, etc.) rely on materials that are subject to confinement and/or finite size effects. How and to what extent the properties of a material—especially a polymer—are changed

under such conditions is a topic of intense debate (*1*–*8*). The ultimate objective is isolated molecules and their properties in comparison to the bulk. Various techniques are available to deposit (*9*, *10*) and to manipulate (*11*) single low–molecular weight polymeric molecules on a surface and to characterize (*12*–*16*) their structure and conformation. In contrast, little is known about the dynamics in such systems as measured in a broad spectral range and at widely varying temperatures. Investigations have been limited to nanometer thin films of low molecular weight (*17*) and polymeric (*1*–*7*, *18*) layers. Here, we report an approach (*8*) that enables the study of both conformation and dynamics of isolated polymer coils by combining atomic force microscopy (AFM) and broadband dielectric spectroscopy (BDS).

Using nanostructured electrode arrangements (*19*) (Fig. 1, A to C), we assembled a capacitor with a separation of 35 nm and isolated polymer coils deposited on one of the electrodes (Fig. 1D and supplementary materials). As a model system, we used poly(2-vinylpyridine) (P2VP), which is known to establish attractive interactions with the native silica on the silicon electrodes. Consideration of the bulk density and the number-averaged molecular weight enables us to estimate the average volume of a single chain, $\hat{V}_{chain}$ (supplementary materials). A comparison with the coils shown in Fig. 1E (close-up and profile) reveals volumes close to $\hat{V}_{chain}$ (left profile, $V \approx 1.8\hat{V}_{chain}$; right profile, $V \approx 0.4\hat{V}_{chain}$). In view of the molecular weight distribution, this diversity of volumes is expected for single chains. The average coil volume corresponds to $0.9\hat{V}_{chain}$, hence on average, there is only one (isolated) P2VP polymer chain per nanodroplet. In the semi-isolated case, we detected volumes equal to $7.8\hat{V}_{chain}$ and $5.1\hat{V}_{chain}$ for two different molecular weights (Table 1).

In BDS measurements, the dynamic glass transition is associated with the so-called α-relaxation (*20*). Our measurements show that this relaxation process is still present in samples containing only isolated condensed polymer chains (Fig. 2). Because they, and similarly semi-isolated agglomerates consisting of ~5 to 10 chains, have a large surface-to-volume ratio, one would expect notable interactions with the supporting substrate, as is the case for thin polymer layers, for which the literature predicts and reports enhancement or reduction (*1*–*3*) of the glassy dynamics (depending on the type of polymer-substrate interaction). Such changes would result in a shift of the α-relaxation with respect to the bulk. Although similar scenarios have been reported (*1*–*3*), the results are contradictory. Several studies found no alteration of the glassy dynamics in thin polymer layers in the linear response regime (*4*–*7*). In our measurements, the maximum position of the α-relaxation in semi-isolated and isolated condensed polymer chains shows (i) a Vogel-Fulcher-Tammann (VFT) temperature dependence (see supplementary materials), which is the characteristic signature of the dynamic glass transition, and (ii) no deviations from the bulk within the experimental uncertainty (Fig. 3). A close look at the α-relaxation peak reveals a broadening in the case of polymer coils relative to the bulk; this is most pronounced in the case of isolated chains (Fig. 2). The dielectric loss spectra normalized with respect to the peak maximum show that this broadening happens almost exclusively on the low-frequency side (Fig. 3, inset). The observed broadening of the α-relaxation peak accounts for 12% of the total

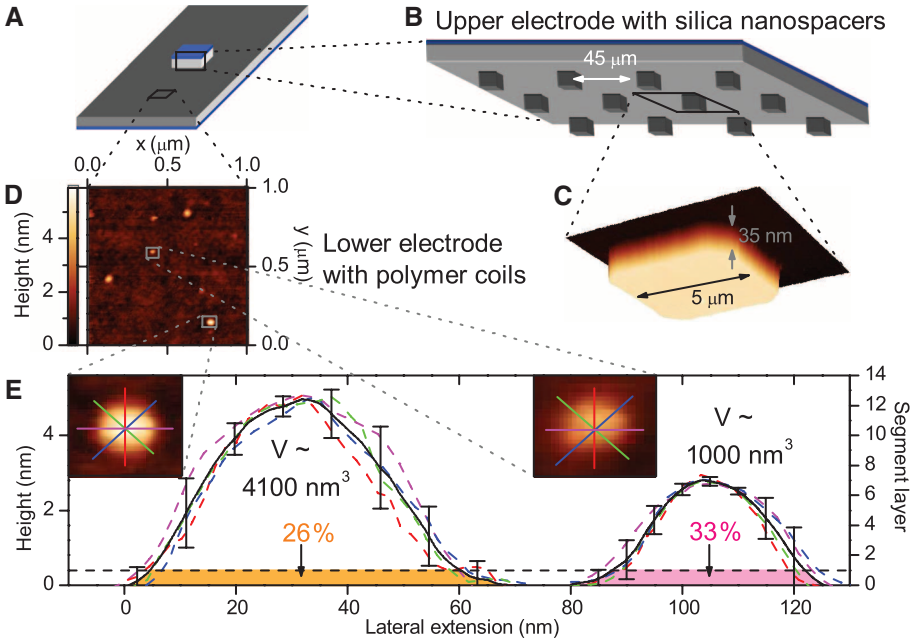

Fig. 1. Sample arrangement required to study condensed (semi-)isolated polymer coils by means of BDS and their topography. (**A**) Two highly doped, conductive silicon electrodes (measures for bottom and top electrode: 4×10 mm^2 and 1×1 mm^2, respectively) are assembled to build the sample capacitor. (**B**) The top electrode has an array of strongly insulating silica nanostructures as spacers on its lower side, which cover about 1% of the surface area. (**C**) Spacers of a height of 35 nm, as shown in this AFM image, were used to conduct measurements of condensed isolated P2VP chains. (**D**) AFM scans of the same sample studied by BDS were taken to analyze the volume of the polymer coils. (**E**) Averaged profiles of two coils from (D) (shown in the close-ups) demonstrate the variation in height, radius, and volume among the coils. The error bars correspond to the standard deviation of the four height profiles as indicated by the colored lines (which are the basis of the averaged profiles); this illustrates a high degree of symmetry within each coil. The percent values give the volume proportion of the layer of chain segments in direct contact with the solid substrate.

Table 1. Specification of the polymers used and mean coil volume analysis of the condensed polymer coils of the samples that have successfully been measured by BDS. The molecular weight and number-average molecular weight (M_W and M_n, respectively) as well as the polydispersity index (PDI) were determined by gel permeation chromatography.

Polymer property	Polymer 1 values	Polymer 2 values	
M_W (kg/mol)	1020	2250	
M_n (kg/mol)	766	1510	
PDI	1.33	1.49	
T_g (K) by DSC	371 (±1)	375 (±1)	
$\hat{V}_{chain}$ (nm^3)	1142	2251	
Chain distribution	Semi-isolated	Semi-isolated	Isolated
$\hat{V}_{coil}$ (nm^3) ± SE	8864 (±2500)	11,564 (±3500)	2033 (±500)
$\hat{V}_{coil}/\hat{V}_{chain}$ ± SE	7.8 (±2.2)	5.1 (±1.6)	0.9 (±0.2)
Coil density (μm^{-2})	37.5	10.0	4.0
Area analyzed (μm^2)	8	8	13.75
Number of analyzed coils	300	80	55

[1]Faculty of Physics and Earth Science, University of Leipzig, 04103 Leipzig, Germany. [2]Max Planck Institute of Microstructure Physics, 06120 Halle (Saale), Germany.

*Corresponding author. E-mail: kremer@physik.uni-leipzig.de

peak area, which is a measure of the number density of the fluctuating molecular dipoles. Therefore, only this proportion of the mobile segments no longer have bulk-like dynamics.

To connect this insight concerning the dynamics to the interfacial topology of the (semi-) isolated polymer coils, the height distribution of the volume is deduced from AFM images. Because two or three monomer segments constitute the structural unit underlying glassy dynamics (*21*), this volume is subdivided into layers, each with a thickness of ~0.4 nm, approximating the width of a P2VP chain (*16*). The most reasonable conjecture is that the segments closest to the solid substrate (Fig. 1E) account for the slower relaxation modes in the case of attractive interactions, as present in the investigated system. The volume fraction of the first layer of segments in direct contact with the solid substrate accounts for 25 to 30% and 15 to 20% of the total coil volume in the cases of isolated and semi-isolated chains, respectively. These proportions are considerably larger than the fraction of slower relaxation modes (~12%), indicating that not all segments that are in direct vicinity of the solid interface contribute to the detected slower dynamics.

Examination of the interactions at the P2VP-silica interface using infrared (IR) spectroscopy revealed that ~50% of the terminal hydroxyl (OH) groups of the silica surface interact with the pyridine ring of the P2VP segments (fig. S3 and supplementary materials). Because the size of a segment is similar to the distance between the OH groups (*22*), we conclude that only about half of the segments in the first layer at the interface are subject to hydrogen bonding. Hence, the amount of broadening found in the BDS data is in accord with the volume fraction of the first segment layer in the polymer coils. However, it remains unknown whether the interacting proportion of segments exhibits the detected slower dynamics, or whether they are completely immobilized and the slower relaxations have to be assigned to those segments neighboring the pinned ones. The latter scenario is suggested by other studies on the adsorption of polymer chains at solid interfaces (*23*).

A cooperative process such as the dynamic glass transition (*24*) can take place even in condensed isolated polymer chains because the length scale on which this fluctuation takes place—which typically corresponds to two or three polymer segments (*21*)—is much smaller than the extension of the coil as a whole (Fig. 3, lower left).

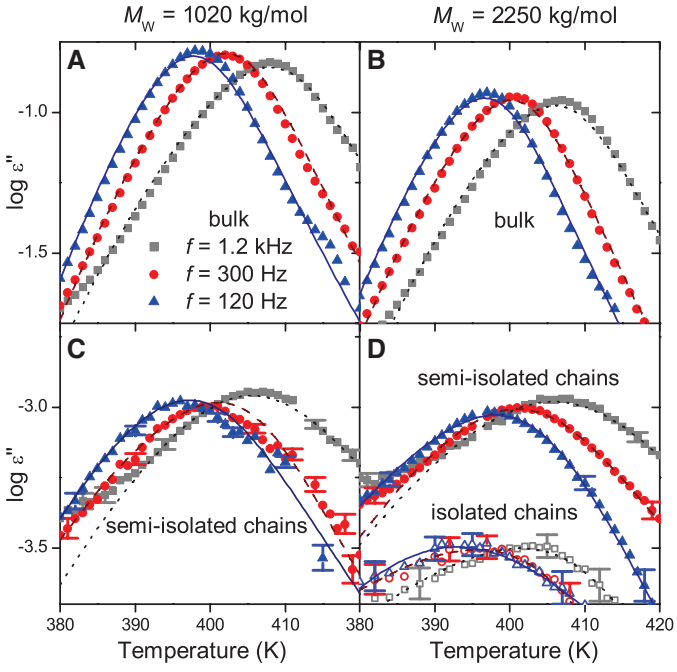

Fig. 2. Dielectric loss ε″ versus temperature for two different molecular weights (labeled at the top of each column) of P2VP bulk, condensed semi-isolated polymer coils and condensed isolated coils at different frequencies as indicated (same symbol shapes denote same frequencies in all panels). (**A** and **B**) In the bulk, the α-relaxation is clearly visible. (**C** and **D**) The same is true in the case of condensed semi-isolated (solid symbols) and even isolated [(D), open symbols)] P2VP polymer chains. The decrease in dielectric strength (signal intensity) in the semi-isolated and isolated coils is due to the much smaller filling fraction of the sample capacitor because ε″ is averaged over the whole capacitor volume. For clarity, a conductivity contribution intrinsic to P2VP was subtracted. In the bulk measurements, the experimental error is smaller than the symbol size; for the other measurements, the error bars correspond to the accuracy of the dielectric measurement system (3×10^{-5}). The dotted, dashed, and solid lines are Havriliak-Negami functions extended with a VFT temperature dependence of the relaxation time τ_{HN} fitted to the data (see supplementary materials).

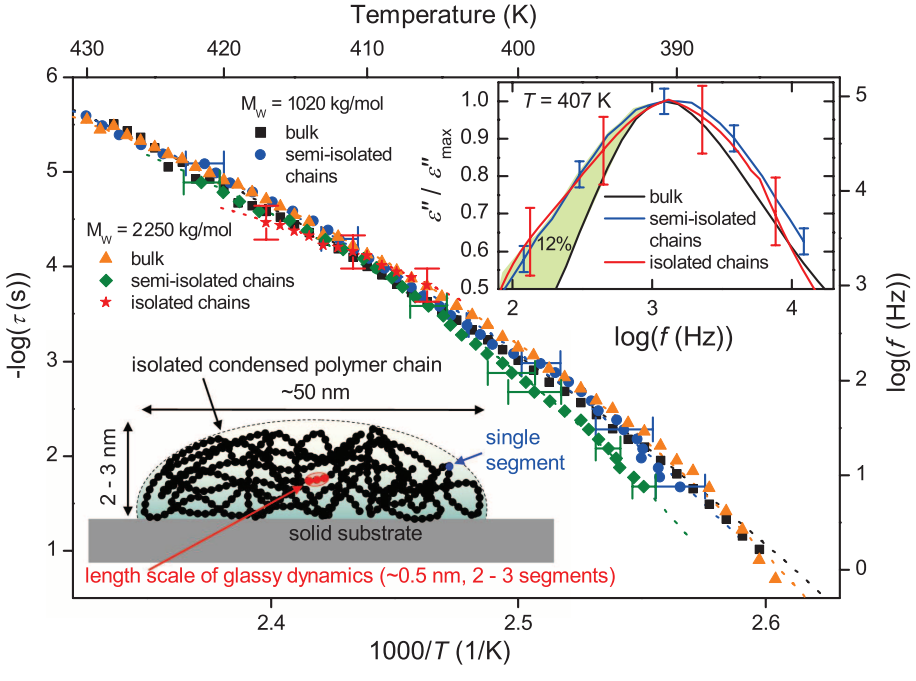

Fig. 3. Activation plot of the α-relaxation of condensed semi-isolated and isolated P2VP polymer coils and the respective bulk dynamics for two molecular weights as indicated. The dotted lines are VFT fits to the data; the error bars indicate the accuracy of the determination of the peak position of the α-relaxation. **Inset:** Dielectric loss spectra (recorded at 407 K) of bulk, semi-isolated chains, and isolated chains normalized by the respective maximum value; the latter two are broadened, especially on the low-frequency side, which corresponds to the occurrence of longer relaxation time modes. In the bulk measurements, the experimental uncertainty is smaller than the line width; for the other measurements, the error bars correspond to the accuracy of the dielectric measurement system (3×10^{-5}). The sketch at lower left illustrates the length scale intrinsic to glassy dynamics in comparison to the size of a single condensed polymer chain.

References and Notes

1. O. K. C. Tsui, T. P. Russell, C. J. Hawker, *Macromolecules* **34**, 5535–5539 (2001).
2. C. J. Ellison, S. D. Kim, D. B. Hall, J. M. Torkelson, *Eur. Phys. J. E* **8**, 155–166 (2002).
3. Y. Koh, G. McKenna, S. L. Simon, *J. Polym. Sci. B* **44**, 3518–3527 (2006).
4. M. Efremov, E. Olson, M. Zhang, Z. Zhang, L. Allen, *Macromolecules* **37**, 4607–4616 (2004).
5. E. U. Mapesa *et al*., *Eur. Phys. J. Spec. Top.* **189**, 173–180 (2010).
6. M. Tress *et al*., *Macromolecules* **43**, 9937–9944 (2010).
7. M. Erber *et al*., *Macromolecules* **43**, 7729–7733 (2010).
8. F. Kremer, E. U. Mapesa, M. Tress, M. Reiche, in *Recent Advances in Broadband Dielectric Spectroscopy*, Y. Kalmykov, Ed. (Springer, Dordrecht, Netherlands, 2013), pp. 163–178.
9. R. B. Salazar, A. Shovsky, H. Schönherr, G. J. Vancso, *Small* **2**, 1274–1282 (2006).
10. M. Jaschke, H.-J. Butt, *Langmuir* **11**, 1061–1064 (1995).
11. C. Acikgoz, M. A. Hempenius, G. Julius Vancso, J. Huskens, *Nanotechnology* **20**, 135304 (2009).
12. J. Kumaki, Y. Nishikawa, T. Hashimoto, *J. Am. Chem. Soc.* **118**, 3321–3322 (1996).
13. J. Kumaki, T. Hashimoto, *J. Am. Chem. Soc.* **125**, 4907–4917 (2003).
14. A. Kiriy, G. Gorodyska, S. Minko, M. Stamm, C. Tsitsilianis, *Macromolecules* **36**, 8704–8711 (2003).
15. M. E. McConney, S. Singamaneni, V. V. Tsukruk, *Pol. Rev.* **50**, 235–286 (2010).
16. Y. Roiter, S. Minko, *J. Am. Chem. Soc.* **127**, 15688–15689 (2005).
17. S. Capponi, S. Napolitano, M. Wübbenhorst, *Nat. Commun.* **3**, 1233 (2012).
18. E. V. Russell, N. E. Israeloff, L. E. Walther, H. Alvarez Gomariz, *Phys. Rev. Lett.* **81**, 1461–1464 (1998).
19. A. Serghei, F. Kremer, *Rev. Sci. Instrum.* **79**, 026101 (2008).
20. F. Kremer, A. Schönhals, Eds., *Broadband Dielectric Spectroscopy* (Springer, Berlin, 2003).
21. I. Bahar, B. Erman, F. Kremer, E. Fischer, *Macromolecules* **25**, 816–825 (1992).
22. C. Iacob *et al*., *Phys. Chem. Chem. Phys.* **12**, 13798–13803 (2010).
23. S. Napolitano, M. Wübbenhorst, *Nat. Commun.* **2**, 260 (2011).
24. G. Adam, J. Gibbs, *J. Chem. Phys.* **43**, 139 (1965).

Acknowledgments: We thank the Leibniz Institute of Polymer Research Dresden (IPF), especially P. Uhlamnn and A. Lederer, for conducting GPC measurements and A. Synytska for helpful discussions. Supported by the Graduate School BuildMoNa (M.T.), a Deutsche Forschungsgemeinschaft (DFG) grant within project SPP 1369 (E.U.M.), and DFG grant SFB TRR 102. A description of the sample preparation and the volume detection of the polymer coils, as well as details on the BDS and IR measurements, can be found in the supplementary materials. F.K. initiated and guided the project; M.R. was responsible for the fabrication of the nanostructured silicon wafers; M.T. and E.U.M. tested the suitability of the silicon wafers and developed the cleaning procedure; M.T. conducted the BDS experiments and AFM measurements, and analyzed the data; W.K.K. produced and filled the silica pores; W.K. performed and analyzed the IR measurements; and M.T., F.K., and E.U.M. wrote the manuscript.

Supplementary Materials

www.sciencemag.org/content/341/6152/1371/suppl/DC1
Materials and Methods
Supplementary Text
Figs. S1 to S3
References (*25*–*37*)

9 April 2013; accepted 14 August 2013
10.1126/science.1238950

Lewis Acidity of Organofluorophosphonium Salts: Hydrodefluorination by a Saturated Acceptor

Christopher B. Caputo, Lindsay J. Hounjet, Roman Dobrovetsky, Douglas W. Stephan*

Prototypical Lewis acids, such as boranes, derive their reactivity from electronic unsaturation. Here, we report the Lewis acidity and catalytic application of electronically saturated phosphorus-centered electrophilic acceptors. Organofluorophosphonium salts of the formula $[(C_6F_5)_{3-x}Ph_xPF][B(C_6F_5)_4]$ (x = 0 or 1; Ph, phenyl) are shown to form adducts with neutral Lewis bases and to react rapidly with fluoroalkanes to produce difluorophosphoranes. In the presence of hydrosilane, the cation $[(C_6F_5)_3PF]^+$ is shown to catalyze the hydrodefluorination of fluoroalkanes, affording alkanes and fluorosilane. The mechanism demonstrates the impressive fluoride ion affinity of this highly electron-deficient phosphonium center.

Phosphorus(III) Lewis bases are widely exploited as ligands in transition metal coordination and organometallic chemistry; however, the electrophilic nature of phosphorus centers has garnered lesser attention. P(III) phosphenium cations have been explored by Gudat, Burford, and Ragogna, among others (*1*, *2*). In recent computational work, phosphenium cations have been predicted to exhibit fluorophilicities comparable to those of known neutral Lewis acids, but substantially weaker than those of electrophilic cations such as $[Me_3Si]^+$ (Me, methyl) (*3*). Although P(V) Lewis acidity has been explored less (*4*), it is noteworthy that the P(V) centers in ylide reagents account for the classic Wittig reactions with ketones (*5*). Similarly, phosphonium cations have been used to facilitate additions to polar unsaturates (*6*) and Diels-Alder reactions (*7*). In related efforts, Hudnall *et al*. have also recently exploited the acceptor capabilities of phosphonium cations, in tandem with boranes, to develop a series of fluoride ion sensors (*8*). Whereas these findings reveal the Lewis acidity of P cations, the chemistry of highly electrophilic phosphonium salts remains unexplored. Targeting such systems, we reported nucleophilic attack of a phosphine donor at an electron-deficient organofluorophosphonium salt (*9*, *10*), leading to the phosphonium-difluorophosphorane product $[Ph_3P(1,4\text{-}C_6F_4)Ph_2PF_2][O_3SCF_3]$ (Ph, phenyl) (*9*). This behavior is reminiscent of the reactivity of $B(C_6F_5)_3$ (*11*), suggesting that $[(C_6F_5)Ph_2PF]^+$ and $B(C_6F_5)_3$ have similar Lewis acidity. Nonetheless, in contrast to the electrophilic nature of borane species, which is derived from the presence of a vacant p orbital, the Lewis acidity of organofluorophosphonium cations resides in the σ* acceptor orbital oriented opposite the fluoride substituent (*12*). Further, the trigonal planar, electronically unsaturated nature of borane Lewis acids make them reactive toward most donor molecules. In contrast, phosphonium cations are electronically saturated and contain a P center that is sterically shielded by a pseudo-tetrahedral arrangement of substituents. As a consequence, most phosphonium salts are unreactive toward electron donors. Herein, the incorporation of electrophilic substituents at P is shown to afford highly Lewis acidic phosphonium centers. As a demonstration of their particularly strong fluorophilicity, these organofluorophosphonium cations are shown to directly activate C–F bonds and to effect the catalytic hydrodefluorination (HDF) of fluoroalkanes.

The electron-deficient phosphines $(C_6F_5)_2PhP$ and $(C_6F_5)_3P$ are cleanly oxidized with XeF_2 to give difluorophosphoranes $(C_6F_5)_2PhPF_2$ (**1**) and $(C_6F_5)_3PF_2$ (**2**) in quantitative yields. These species exhibit triplet resonances in their $^{31}P\{^1H\}$ nuclear magnetic resonance (NMR) spectra at chemical shifts [δ/parts per million (ppm)] –54.8 and –48.0, respectively, with a one-bond coupling constant ($^1J_{PF}$) of ~695 Hz. In contrast to the more electron-rich difluorophosphorane $(C_6F_5)Ph_2PF_2$ (*13*), neither **1** nor **2** undergoes fluoride ion abstraction by the Lewis acids $B(C_6F_5)_3$ or Me_3SiOTf (OTf, trifluoromethanesulfonate) (*9*, *10*), leading to our inference that the targeted fluorophosphonium cations should exhibit comparatively stronger Lewis acidity. Nevertheless, **1** and **2** both undergo fluoride ion abstraction by $Al(C_6F_5)_3{\cdot}C_7H_8$ (*14*) or $[Et_3Si][B(C_6F_5)_4]{\cdot}2C_7H_8$ (Et, ethyl) (*15*, *16*) to generate the corresponding fluorophosphonium salts $[(C_6F_5)_2PhPF]X$ {X = $[F(Al(C_6F_5)_3)_2]$, **3**; $[B(C_6F_5)_4]$, **4**} and $[(C_6F_5)_3PF]X$ {X = $[F(Al(C_6F_5)_3)_2]$, **5**; $[B(C_6F_5)_4]$, **6**}, respectively (Fig. 1). Products **5** and **6** were easily identified by distinctive doublet resonances in their $^{31}P\{^1H\}$ NMR spectra at δ 77.7 ($^1J_{PF}$ = 1042 Hz) and 67.8 ($^1J_{PF}$ = 1062 Hz) and in their ^{19}F NMR spectra at δ –121.9 (doublet of pentets, $^1J_{PF}$ = 1042 Hz) and –120.5 (doublet of septets, $^1J_{PF}$ = 1062 Hz), respectively. The x-ray structure of **3** (Fig. 2A) clearly reveals the tetrahedral geometry of the

Department of Chemistry, University of Toronto, 80 St. George Street, Toronto, Ontario M5S 3H6, Canada.

*Corresponding author. E-mail: dstephan@chem.utoronto.ca